LAWRENCE
LIVERMORE
NATIONAL
LABORATORY

LLNL-JRNL-508473

Nearly Equivalent Inter- and Intramolecular Hydrogen Bonding in 1,3,5-Triamino-2,4,6-trinitrobenzene at High Pressure

M. R. Manaa, L. E. Fried

October 25, 2011

Journal of Physical Chemistry C

Disclaimer

Nearly Equivalent Inter- and Intramolecular Hydrogen Bonding in 1,3,5-Triamino-2,4,6-trinitrobenzene at High Pressure

M. Riad Manaa* and Laurence E. Fried

Lawrence Livermore National Laboratory, Energetic Materials Center, Livermore, CA, 94551

Journal of Physical Chemistry C

* Corresponding author, email: manaa1@llnl.gov

Abstract

We report density functional theoretical calculations of the equation of state (EOS) of 1,3,5-triamino-2, 4,6-trinitobenzene (TATB) under hydrostatic compression of up to 250 GPa. Our results show increasing bond equivalency between the intramolecular and intermolecular hydrogen bonds of the amino and nitro groups in the region 30<P<70 GPa, beyond which the difference between the two bond distances remains constant. This approximate bond equivalency is manifested by a rapid decrease of the intermolecular -NO---HN- distance along the b lattice direction from 2.6 Å at the zero pressure equilibrium geometry to 1.72 Å at 67 GPa, and by a decrease of the intramolecular -NO---HN- bond from 1.65 Å to 1.57 Å for the same pressure region. The strengthening of intermolecular hydrogen bonding with increased pressure is in accordance with recent infrared spectroscopic measurements of decreasing activity of NH_2 vibrational modes with increasing pressure up to 40 GPa.

I. Introduction

Hydrogen bonding plays a fundamental role in defining the unique chemical and physical characteristics of many compounds, such as ice, water, and nucleic acid base pairs. Under conditions of extreme pressure and/or temperature, hydrogen bonds can be profoundly changed through the process of bond symmetrization. In symmetric hydrogen bonding, the covalent X–H bond becomes identical to the intermolecular X---H bond, where X is an electronegative element or an electron acceptor group. Recent examples include the discovery of a polymeric phase in solid formic acid,[1,2] the emergence of symmetric hydrogen bonding in superionic water at 2000 °K and 95 GPa,[3] in HF at 900 °K and 66 GPa,[4] and in solid HBr at 100 °K and pressure up to 40 GPa.[5] Some compounds exhibit both intramolecular X—H hydrogen bonds, and intermolecular X—H hydrogen bonds. The response of intramolecular X—H hydrogen bonds to conditions of extreme pressure has not been extensively studied.

The energetic molecular solid TATB (1, 3, 5-triamino-2, 4, 6-trinitrobenzene) could manifest interesting X---H hydrogen bonding changes at elevated pressure. TATB is known to have extraordinary insensitivity to thermal, impact or shock insults.[6] TATB has one well established polymorph, a triclinic centro-symmetric crystal structure with two molecules per unit cell.[7] This structure is reminiscent of the graphitic sheets of carbon. TATB exhibits significant inter- and intramolecular hydrogen bond interactions, which are thought to be responsible for its almost complete insolubility in most common solvents.[8,9] In crystal TATB, the intermolecular oxygen-hydrogen bond along the b lattice vector is about 2.5 Å, while the intramolecular bond distance is 1.65 Å (see figure 1) at ambient conditions. Ab initio calculations showed that there are relatively large rotational

and torsional barriers for the nitro group, approximately 11 and 6 kcal/mol, respectively, in molecular TATB,[10,11] and that the hydrogen bonding interaction is about 5 kcal/mol along the *a* crystallographic direction.[12,13] These results are indicative of strong intra- and intermolecular hydrogen bonding. It is likely that these hydrogen bonds will strengthen under pressure. This scenario is supported by decreasing IR peak frequencies of the NH_2 symmetric and antisymmetric modes with increasing pressure of up to 10 GPa.[14]

There have been several experimental studies of TATB under hydrostatic pressure, most of which were limited to pressures less than 15 GPa. Stevens et al. used powder X-ray diffraction in conjunction with diamond anvil cell and determined the pressure-volume (*P-V)* isotherm up to 13 GPa.[15] They found lower compressibility of TATB as compared to an earlier experiment,[16] and a subtle cusp in the isotherm at ~8 GPa, the origin of which could not be ascertained. Stevens et al. hypothesized a possible dimerization based on similar results in other systems such as TNT and anthracene. Pressure-dependent coloration of TATB from yellow to red in the pressure region of 2.6-18 GPa was observed, although its cause is still unknown.[15,17] Raman scattering of TATB up to 16 GPa and IR spectra up to 10 GPa did not show any evidence for pressure-induced phase transition or chemical reactivity.[14, 18] The single-pulse Raman scattering spectrum of *shocked* TATB, however, revealed a new, very weak vibrational band above 7 GPa.[19] Recently, Pravica et al.[20] extended their previous synchrotron infrared measurements in the mid and far IR spectral region up to 40 and 30 GPa, respectively. They found that most of the spectral lines steadily increased in frequency with pressure except for the NH_2 symmetric and antisymmetric vibrations near 3220 and 3320 cm^{-1},

which steadily decreased with increasing pressure, presumably due to an increase in intermolecular hydrogen bonding upon compression.

Several density functional theoretical (DFT) studies have also been conducted on TATB subjected to hydrostatic compression. An elaborate study on TATB (and other energetic molecular solids) up to 7 GPa employed different functionals and plane wave basis set sizes. The simulations predicted a softer *P-V* curve than was found in experiments, irrespective of the employed methodology, although the inaccuracy in the compressibility diminished as pressure increased. This was attributed to the inadequate treatment of van der Waals interactions within DFT.[21] A comparative DFT study of up to P=10 GPa obtained a *P-V* curve in better agreement with experiment from the local density approximation (LDA) than from the generalized gradient approximation (GGA).[22] Two recent DFT studies with an empirical van der Waals (vdW) correction were in much better accord with the experimental results up to 7 GPa,[23] and 30 GPa.[24] It was noted that the inadequate treatment of hydrogen bonding is problematic even in vdW-DFT calculations of TATB, because of its in-plane hydrogen bond interactions.[24] Finally, the DFT-LDA study of Wu et al. of TATB under uniaxial compression determined the onset of metallization at 120 GPa.[25]

In this work, we use pure (i.e. without a vdW correction) spin-polarized DFT calculations to study the hydrostatic compression of TATB up to 250 GPa. Our calculations provide an equation of state for unreacted TATB that is in good agreement with experimental determination. We also find a high-pressure region in which both intramolecular and intermolecular hydrogen bonds become almost equivalent, a manifestation of strong intermolecular hydrogen bonding upon compression that is in

accord with recent spectroscopic measurements.

II. Computational Approach

Calculations were performed on a unit cell of TATB crystal ($P\bar{1}$ symmetry group), which contains two molecules (a total of 48 atoms). We used the spin-polarized generalized gradient corrected approximation of Perdew–Burke–Ernzerhof (PBE) for the exchange-correlation potential.[26] Spin polarization was included to account for any possible pressure – induced bond breaking or formation. Previously, a study of nitromethane under pressure found that uniaxial compression of about 25–40 GPa along the b lattice vector caused the C–H bond to be either highly stretched or dissociated, with a similar outcome under isotropic compression at much higher pressures.[27] In our work, electron–ion interactions were described by Vanderbilt-type ultrasoft pseudopotentials,[28] and orbitals were expanded in a plane wave basis set. We chose a plane wave basis with a kinetic energy cutoff of 380 eV, since others found that a similar choice gave the best agreement with the experimental equilibrium geometry on four energetic molecular crystals.[29] The pure DFT calculations of Byrd and Rice showed that volumes based on both the PW91 and PBE functionals converge to the same values as pressure increases (up to 6-7 GPa) regardless of whether a planewave basis set cut-off of 396 545 eV was used. [21] We also note that the pure DFT work of Byrd et al. [29] utilized planewave cut-offs ranging from 280 to 800 eV to calculate the equilibrium geometry of four energetic molecular crystals. They found that the difference between experimental and computed volumes did not necessarily decrease with increasing the basis set size, and that the basis set with cut-off ~ 400 eV "fortuitously" produced almost exact agreement with the experimental lattice vectors. While we expect the vdW- corrected DFT calculations to

provide much better results below P=10 GPa than pure DFT, the performance of our pure DFT calculations should be of similar quality in the pressure region of interest to this work, above 30 GPa.

We used 4 k-points in the Brillouin zone, and the minimization procedure used the charge density mixing scheme.[30] A force tolerance of 0.05 eV/Å was used, and the self-consistent field convergence criterion was set to 2 x 10^{-6} eV per atom. Optimizations of compressed cells to the pre-specified external pressure with complete relaxation of atomic coordinates and all lattice parameters were performed at this level of theory using the CASTEP program from MSI.[31]

III. Results and Discussion

Our main objective in this work is to examine the behavior of hydrogen bonding in TATB at high-pressure. Nonetheless, we begin by comparing our results for the equilibrium properties (zero-pressure) and hydrostatic *P-V* isotherm with available experimental and computational studies in the low-pressure region (P < 15GPa), and then proceed to discuss our high-pressure results.

First, complete optimization of the unit cell provided the structure parameters reported in Table I, and are compared with the two x-ray experimental results (Exp1 and Exp2) and three computational results of pure [DFT (2)] [21] and vdW corrected DFT calculations [DFT(3) and DFT(4)].[23,24] Our computed lattice angles (α, β, and γ) show very good agreement with the experimental determination of Cady and Larson (Exp1)[7] with less than 1° deviation. Comparison with the experimental determination of Stevens et al.[15] shows less than 1.2° deviation for β and γ, but 2.8° deviation for α. It is not clear

why the two experimental results give more pronounced deviation for this particular angle. The computed values of pure and corrected DFT (2) and DFT (3) show similar deviations from experiment. We find significant deviation from both experimental results for the lattice parameters *a*, *b*, and *c*, although much less than the pure DFT calculations of Byrd and Rice.[21] The DFT (3) and DFT (4) results, despite the empirical treatment of vdW interactions, show much better agreement with the experimental values. We also note that a pure DFT study on several other weakly bound energetic molecular solids, such as HMX, RDX, and CL20, showed over 9% error in the equilibrium cell parameters, probably because of the neglect of dispersion forces.[29]

Figure 2 shows the calculated *P-V* isotherm up to 18 GPa (Fig.2a) along with previous experimental and computational results, and reports the isotherm for the entire pressure range (Fig.2b) of up to 250 GPa. We note that the calculated EOS in Fig.2a is stiffer than both experimental and computational data up to 2 GPa, while it shows good agreement with the experimental results of Olinger and Cady in the region 3-7 GPa, the highest pressures considered in their study.[16] Considering the earlier pure DFT computational results of Byrd and Rice,[21] the deviation of our results in this pressure range from the experimental determination is most probably due the neglect of vdW forces. The recent vdW-DFT corrected results of Budzevich et al. [24] and Sorescu and Rice [23] showed excellent agreements with the experimental results of Olinger and Cady [16] in the pressure range of 0-7 GPa. The inclusion of spin-polarization and different convergence criteria may account for better agreement of our results with the both vdW-DFT corrected and the experimental *P-V* isotherm of Olinger and Cady for P = 3-7 GPa.

The discrepancy between the two experimental *P-V* isotherms is noteworthy. The stiffness in the *P-V* measurements recorded by Stevens et al.[15] was attributed to biased assumptions made in the earlier experimental data of Olinger and Cady. It was noted that the latter study reported only four diffraction peaks at pressures higher than 3 GPa, which is insufficient to obtain direct determination of the lattice parameters required for the triclinic unit cell of TATB. Further, Stevens et al. noted that in the earlier measurements, two assumptions were made about the compressibility of TATB, which may have biased the results. The first was that the ratio of the lengths of the crystallographic axes *a* and *b* remained constant, and the second was that the graphitic-like sheets were assumed not to shear with respect to one another, making their analysis biased toward the *c* axis. In the recent vdW-DFT corrected study, however, Budzevich et al.[24] concluded that these were reasonable assumptions. Their calculations found that the *a*/*b* ratio changed less than 0.1% up to V/V_0=0.60, which our calculations also confirm (see Fig.3a), and that molecules on two adjacent planes rotate by at most 0.07° with respect to each other under a pressure of 24.2 GPa, which negates the possibility of any shear.

We determined the bulk pressure modulus (B_0) and its pressure derivative (B_0') by fitting our calculated *P-V* compression data to the third-order Birch-Murnaghan equation of state (EOS):[32]

$$P = \frac{3B_0}{2}\left[\vartheta^{7/3} - \vartheta^{5/3}\right] \times \left[1 + \frac{3}{4}(B_0' - 4)\left(\vartheta^{2/3} - 1\right)\right],$$

where $\vartheta = \frac{V_0}{V}$, and $B_0 = -V\left(\frac{\partial P}{\partial V}\right)$. We used a value of V_0 = 503 Å^3 per unit cell in our fits. Since the lowest pressure point in our calculations is 0.7 GPa, we used a linear extrapolation of the lowest two pressure points in our calculations to obtain this V_0 value.

We fit our data in two pressure ranges. Up to P=18 GPa, we found B_0= 12.34 ± 0.95GPa and $B_0' = 5.45 \pm 0.44$ while fitting of our entire *P-V* curve up to 250 GPa yielded B_0= 13.10 ± 0.23 GPa and $B_0' = 5.91 \pm 0.06$. The fitted data are shown as the solid line in Figures 2(a) and (b). These results are compared with similar experimental and computational fits in table II.

Figures 3 and 4 report the calculated lattice constants *a*, *b* (Fig.3a), *c* (Fig.3b), α (Fig.4a), β (Fig.4b), and γ (Fig.4c) as a function of pressure. The lattice constants *a* and *b* in Fig.3a show an almost identical decrease with increasing pressure from around 9.2 to 7.55 Å, about 18% reduction from the equilibrium geometry of both constants at 250 GPa. Our reported values seem to be in reasonable agreement with recent calculations. For example, we find *a*=8.82 Å and *b*=8.81 Å at P=8.2 GPa, and *a*=8.56 Å and *b*=8.58 Å at P=22.0 GPa, compared with the vdW-DFT corrected results of *a*=8.72 Å and *b*=8.74 Å at P=8.0 GPa, and *a*=8.48 Å and *b*=8.52 Å at P=22 GPa.[24] It should be noted that the vdW-DFT corrected calculations showed good agreement of all three constants with the experimental parameters of Olinger and Cady, albeit with a slight deviation for P=7.0 GPa.

The pressure dependence of the *c* lattice constant in Fig.3b exhibits several features. First, this constant experiences a reduction of about 40% at P=250 GPa from its corresponding equilibrium value, more than double that experienced by the *a* and *b* parameters. This indicates that TATB is more compressible along the *c* axis than along the a and b axes, even at pressures above 100 GPa. The vdW-DFT corrected calculations with uniaxial compression along the *a* and *b* axis showed much higher stresses than compressions that reduce the TATB inter-planar distance along the *c* direction.[24] These

calculations also showed that compressions that do not involve deformations along the *c* lattice vector undergo the greatest change in energy per atom upon uniaxial compression. This was attributed to the fact that compression within the *a*-*b* plane significantly compresses the molecules.

Second, we note the appearance of a cusp in the *P*-*V* curve around 13 GPa. A subtle cusp in the *P*-*V* isotherm and its corresponding U_s-U_p Hugoniot was indicated in the experiments of Stevens et al.[15] at approximately 8 GPa, the origin of which was hypothesized to be a possible dimerization of TATB, based on comparison with similar aromatic systems such as benzene and graphite. Our results do not show any tendency of TATB toward dimerization, nor a change from forces primarily van der Waals in nature to covalent character is taking place at this relatively low pressure, as will soon be discussed. Instead, we note that our observed cusp in the *c* lattice constant at a similar pressure is also accompanied by a dramatic increase in α, the angle between the *b* and *c* lattice vectors, of almost 8° and reaching a deviation of about 10° at about 11 GPa. These two observations indicate the tendency of the TATB molecules to realign in order to maximize their interactions in this lower pressure range. Third, we note that the largest differences between our calculated values and those from the vdW-DFT corrected ones are for c and for the angle α. As shown in table I, our calculated *c* value of the equilibrium structure is 0.35 Å above the experimental value. The *c* and α may be more sensitive to van der Waals interactions than other cell parameters.

We find that the *c* parameter undergoes a dramatic reduction near P = 70 GPa. The *a* and *b* cell parameters, however, do not undergo abrupt changes. The sudden change in *c* indicates a transition to stronger interaction between the graphitic planes.

After the transition, the planes are close enough to allow interplanar hydrogen bonding. Referring to Fig.2b, we note that the volume does not undergo a sudden transition near 70 GPa. This indicates that the change in the cell geometry is most likely a second order, or displacive, phase transition.

The pressure dependence of the three lattice angles is displayed in Figure 4 a-c. Despite the large pressure range considered, all three angles seem to reach a plateau in the pressure range of 80-250 GPa. The angle γ shows little change, oscillating between 120° and 120.9° in the entire pressure range. The β angle shows an increase from around 92° to 98° below a pressure of 12 GPa, followed by a decrease to 95° in the region between 12 and 70 GPa, to a plateau near its equilibrium value of around 91° between 80 and 250 GPa, marking about 7° variation for the entire region. As noted above, the most pronounced variation is seen in the α angle: An increase from near 107° to over 119° is observed from the 0-70 GPa region, a dramatic, non monotonic, increase of up to 12°, and a plateau around 116° between 80 and 250 GPa. In contrast, the vdW-DFT corrected results of Budzevich et al.[24] showed a very near constant behavior of γ at around 120° for pressure up to 27 GPa, consistent with our results. However, our results differ in that they reported a near constant trend for β at around 92°, while a qualitative agreement is noted with their most pronounced, monotonic increase of α from around 108° to 113° within the same pressure region.

Our calculated pressure dependence of the intra- and intermolecular hydrogen bond lengths are displayed in Figure 5. The intermolecular hydrogen bond lies approximately along the *b* lattice direction. The intramolecular bond between the hydrogen of the amino and oxygen of the nitro groups undergoes a monotonic decrease

from about 1.65 Å at the equilibrium geometry to 1.57 Å at P=67 GPa, a change of 0.08 Å. For the same pressure range, the intermolecular oxygen-hydrogen bond on adjacent molecules undergoes a more dramatic change from 2.6 Å to 1.72 Å, a change of 0.88 Å. At 67 GPa, the intermolecular bond is only 0.15 Å larger than the intramolecular one, clearly indicating nearly complete equivalency between inter- and intramolecular hydrogen bonds and strong intermolecular interactions within this pressure region. These calculations also indicate that intermolecular compressibility along this direction is more prevalent than intramolecular bond compression. Increasing the pressure from 67 GPa to 250 GPa further decreases both bonds by an equal amount of 0.24 Å. This indicates a persisting resistance towards further bond equivalency. It should be noted that at P=35 GPa, the intermolecular bond length is 1.85 Å, much shorter than a non-covalent N-O…H bond distance. For example, the N-O—H distance is well below the sum of the van der Waals radii (2.62 Å), or the average intermolecular NO…H bond distance of 2.30 Å as determined for various nitro-containing compounds.[33] At this pressure, the intramolecular hydrogen bond length is 1.62 Å, only 0.23 Å shorter than the inter-molecular one. Therefore, we expect that within the region of 30<P<70 GPa TATB should exhibit approximate hydrogen bond equivalency. Indeed, the complex behavior noted by Pravica et al.[20] in their mid-IR (~3000 cm^{-1}) spectral region of the NH_2 symmetric and antisymmetric stretches around 30 GPa may well be due to the manifestation of this incomplete bond equivalency. It is in this pressure region where the NH_2 vibrations are now experiencing strong perturbations from increased contributions of both inter- and intramolecular -NO_2—H_2N- interactions.

Other notable structural changes involve increased puckering of the benzene rings as evidenced in changes of the torsional carbon bonds within a TATB molecule. The torsional angle increases from about 2° to 6° and 8° upon increasing pressure from P~1→ 63→ 240 GPa, respectively. The predicted structure of TATB at 240 GPa is shown in Fig.6. In Fig.6a we have shown the inter-planar hydrogen bond interactions that distinguish the structure over 70 GPa along the *c* lattice, and Fig.6b shows both the intra and inter molecular hydrogen bonds along the *b* direction at the same pressure. We find a pronounced decrease in the interlayer hydrogen – oxygen intermolecular bonds along the *c* lattice vector. At the zero pressure geometry, the shortest distance between a hydrogen of the amine group on one layer and an oxygen of the nitro group along the *c* axis is 3.21 Å. This bond length decreases to 2.51 Å and 2.18 Å when the pressure increases to 63 GPa and up to 240 GPa, respectively. We do not observe any tendency towards pressure-induced chemical transformations within the wide range of this pressure range. This resistance to pressure-induced chemistry may help explain the high degree of insensitivity of TATB.

IV. Conclusion

We conducted spin-polarized DFT calculations on the hydrostatic compression of TATB up to an extreme pressure of 250 GPa. Our calculations showed that the intra and intermolecular -NO_2—H_2N- hydrogen bonds become nearly equivalent at a pressure of 67 GPa. This incomplete bond equivalency progresses monotonically from P > 30 GPa, but increasing pressure beyond 70 GPa up to 250 GPa does not show any added effect. It is expected that vibrational motions involving the NO—HN modes are sensitive to the nearly equivalent hydrogen bonding, as recent spectroscopic IR analysis of the NH_2

stretches revealed. Further, our calculated EOS provided a bulk pressure modulus B_0 = 13.10 GPa and its derivative $B_0' = 5.91$, in reasonable agreement with experimental results recorded up to 7 GPa.[16] Our calculations argue against the possibility of TATB dimerization at a pressure of around 8 GPa, as has recently been hypothesized.[15]

Around 70 GPa, there is a displacive phase transition to a configuration with reduced inter-plane distances. The new phase retains the molecular structure of TATB, although it is characterized by inter-plane hydrogen bonding and subtle ring puckering.

Acknowledgments:

This work is performed under the auspices of the U.S. Department of Energy Lawrence Livermore National Laboratory under Contract DE-AC52-07NA27344. Support from the Advanced Strategic Computation (ASC) program is greatly acknowledged.

Figure Captions:

Figure 1. Measured inter- and intramolecular hydrogen bonds at ambient conditions in a supercell of crystalline TATB along the *b* lattice direction.

Figure 2. P-V hydrostatic isotherm of TATB as determined in (a) this work [DFT (1)] up to 18 GPa, experimental results from Ref.15 (Exp2) and Ref.16 (Exp3), and computational results of pure DFT from Ref.21 [DFT (2)] and vdW-corrected DFT from Ref.23 [DFT (4)], (b) this work up to 250 GPa. Solid lines in (a) and (b) are fits to the Birch-Murnaghan EOS.

Figure 3. Calculated pressure dependence of TATB lattice parameters. (a) The *a* and *b* parameters, and (b) the *c* parameter. Not all data points are shown as symbols.

Figure 4. Calculated pressure dependence of lattice angles (a) α, (b) β, and (c) γ. Not all data points are shown as symbols.

Figure 5. Calculated pressure dependence of inter and intramolecular hydrogen bond lengths. Not all data points are shown as symbols.

Figure 6. The structure of TATB at P = 240 GPa is shown. (a) The inter-plane hydrogen bond in the *c* lattice direction, and (b) inter and intra molecular hydrogen bonds along the *b* direction.

Table I. Comparison of experimental and computational unit cell lattice parameters of TATB crystal.

Parameter [a]	DFT(1)[b]	Exp1.[c]	Exp2.[d]	DFT(2)[e]	DFT(3)[f]	DFT(4)[g]
a	9.219	9.010	8.967	9.364	9.0213	9.077
b	9.181	9.028	9.082	9.369	9.0395	9.087
c	7.161	6.812	6.624	7.505	6.6164	6.693
α	107.7	108.58	110.5	107.2	109.20	111.82
β	92.0	91.82	93.0	91.8	91.81	91.56
γ	120.2	119.97	118.9	120.2	119.93	119.97

[a] Cell dimension in Å and angles in degree.

[b] Current work: DFT(GGS-PBE).

[c] Exp1: Experimental x-ray from Ref. 7.

[d] Exp2: Experimental x-ray from Ref. 15.

[e] DFT(GGA-PW91) of Ref. 21.

[f] DFT+vdW of Ref. 24.

[g] DFT+vdW of Ref. 23.

Table II. Comparison of bulk pressure modulus (B_0) and its pressure derivative (B_0') from various EOS fits.

Parameter	This work [a]	Exp1.[b]	Exp2.[c]	DFT(3) [d]	DFT(4) [e]
B_0*(GPa)*	12.34 (13.10)	16.7	13.6 (17.1)	18.7	12.43
B_0'*(GPa)*	5.45 (5.91)	5.7	12.4 (8.1)	7.9	11.4

[a] This work; Birch-Murnaghan P-V fit using pressures up to 8 GPa .. A fit using pressures of up to 250 GPa is in parenthesis.

[b] Exp1: Experimental results from Ref. 16.

[c] Exp2: Birch-Murnaghan fit to experimental x-ray below 8 GPa from Ref. 15. A fit at pressures up to 13 GPa is in parenthesis.

[d] DFT+vdW of Ref. 24.

[e] DFT+vdW of Ref. 23.

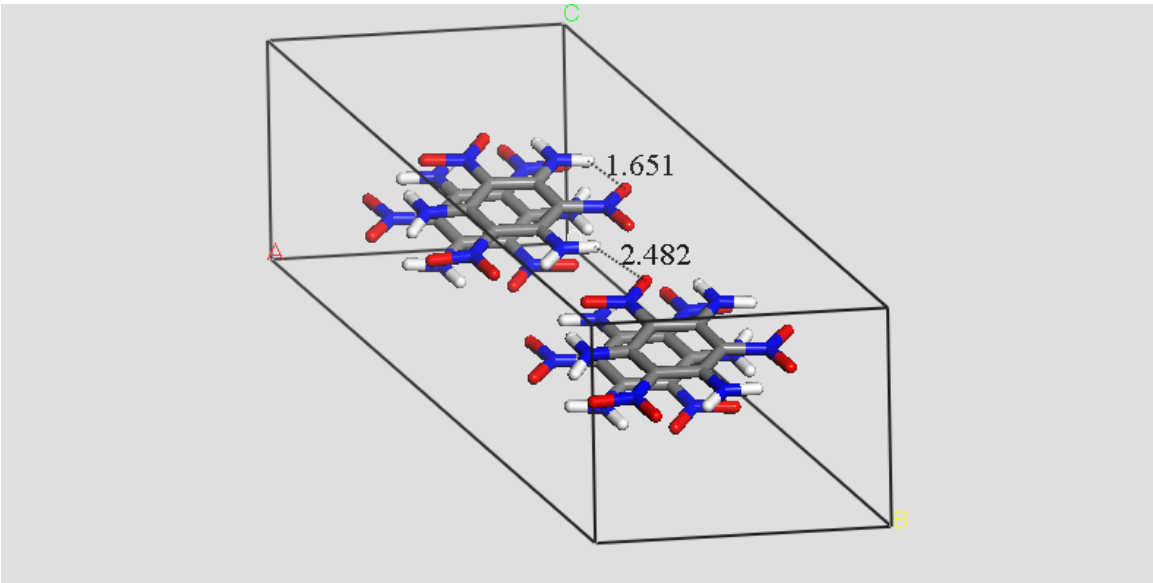

Manaa and Fried: Figure 1.

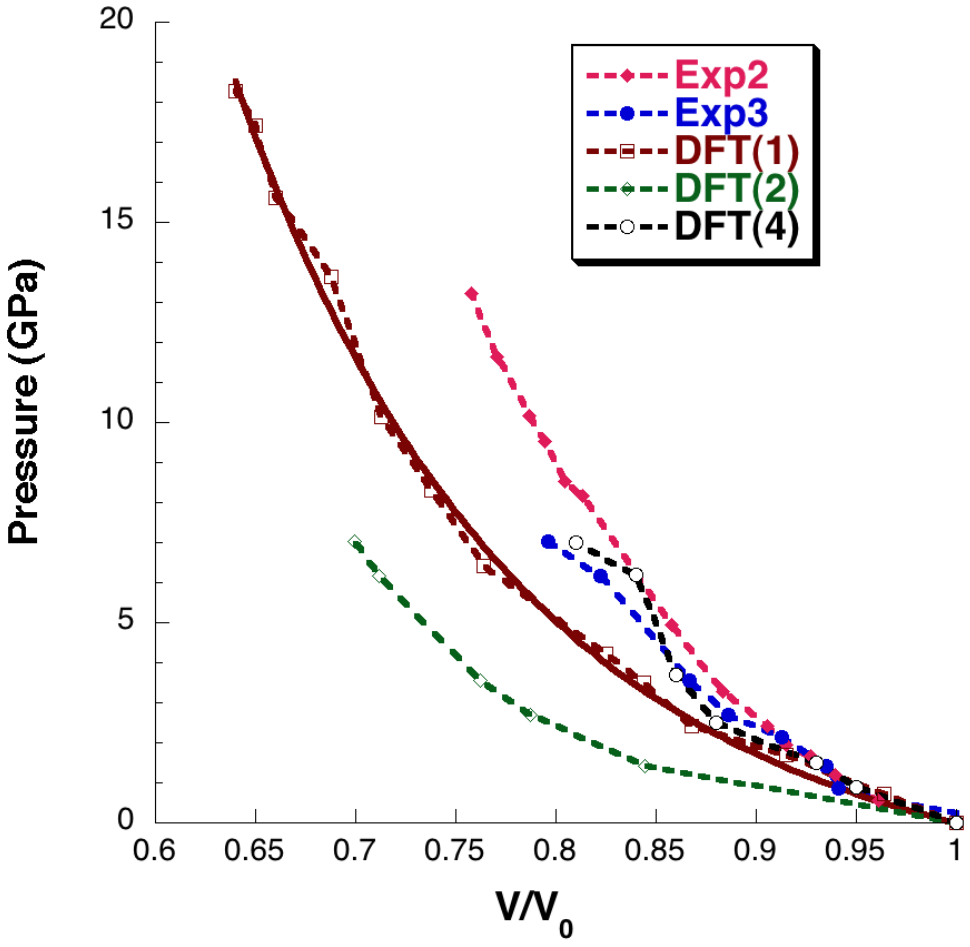

Manaa and Fried: Figure 2(a).

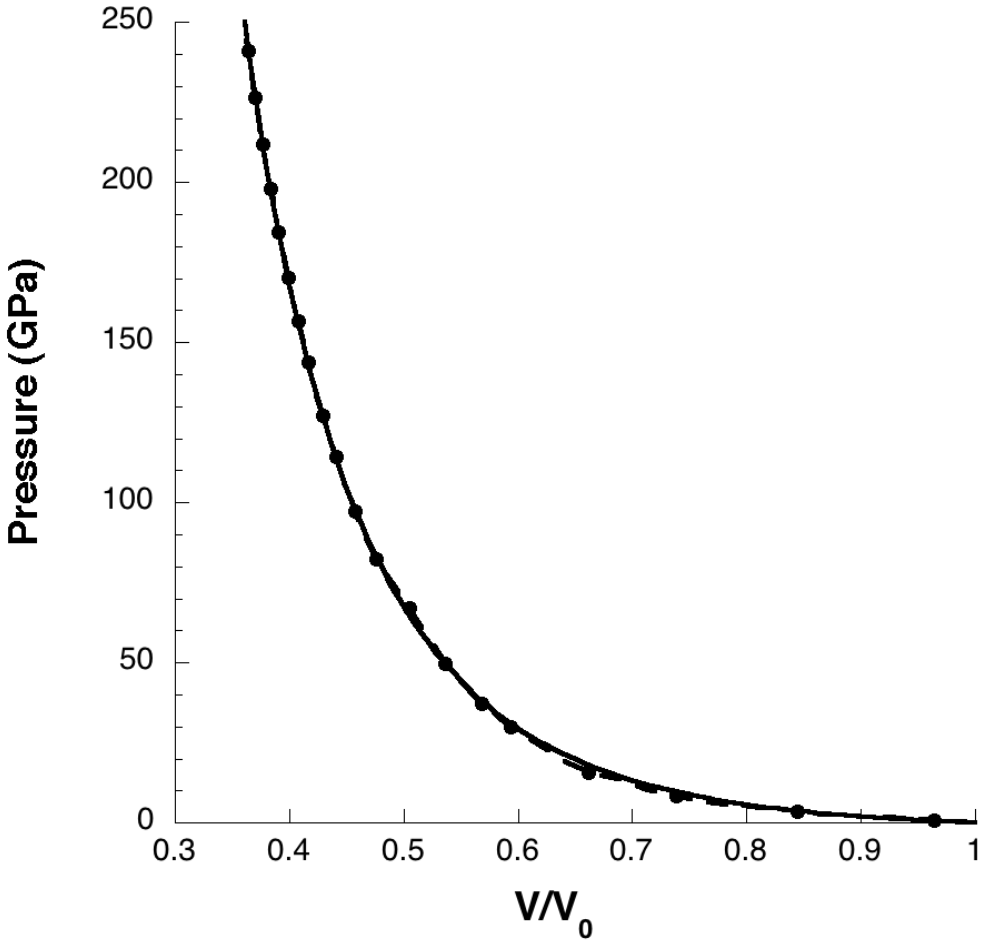

Manaa and Fried: Figure 2(b).

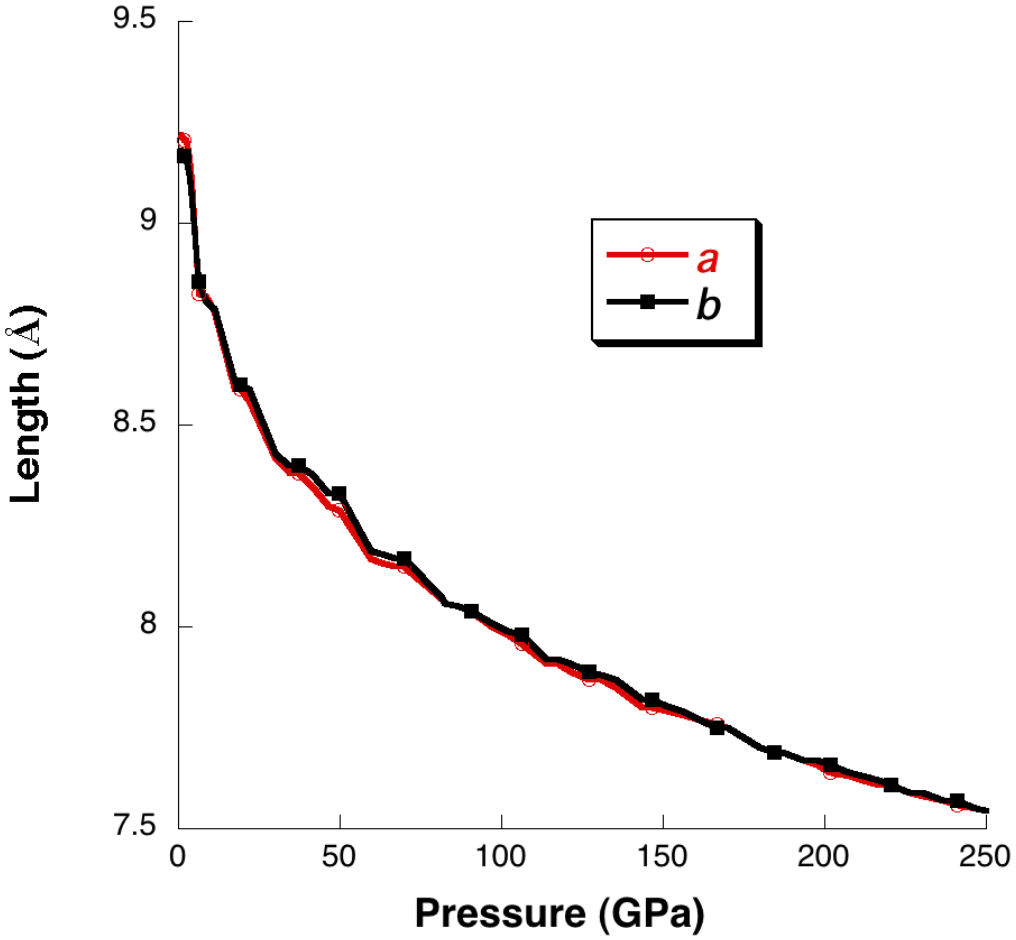

Manaa and Fried: Figure 3 (a).

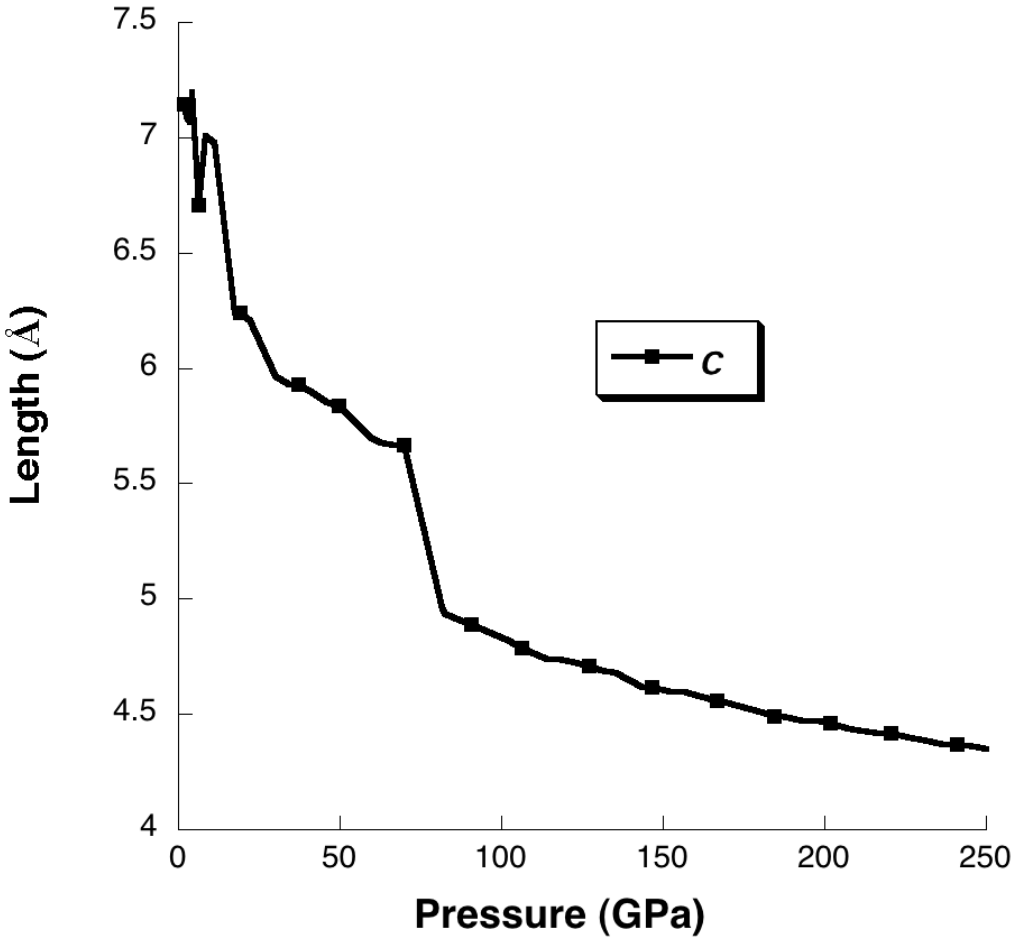

Manaa and Fried: Figure 3 (b).

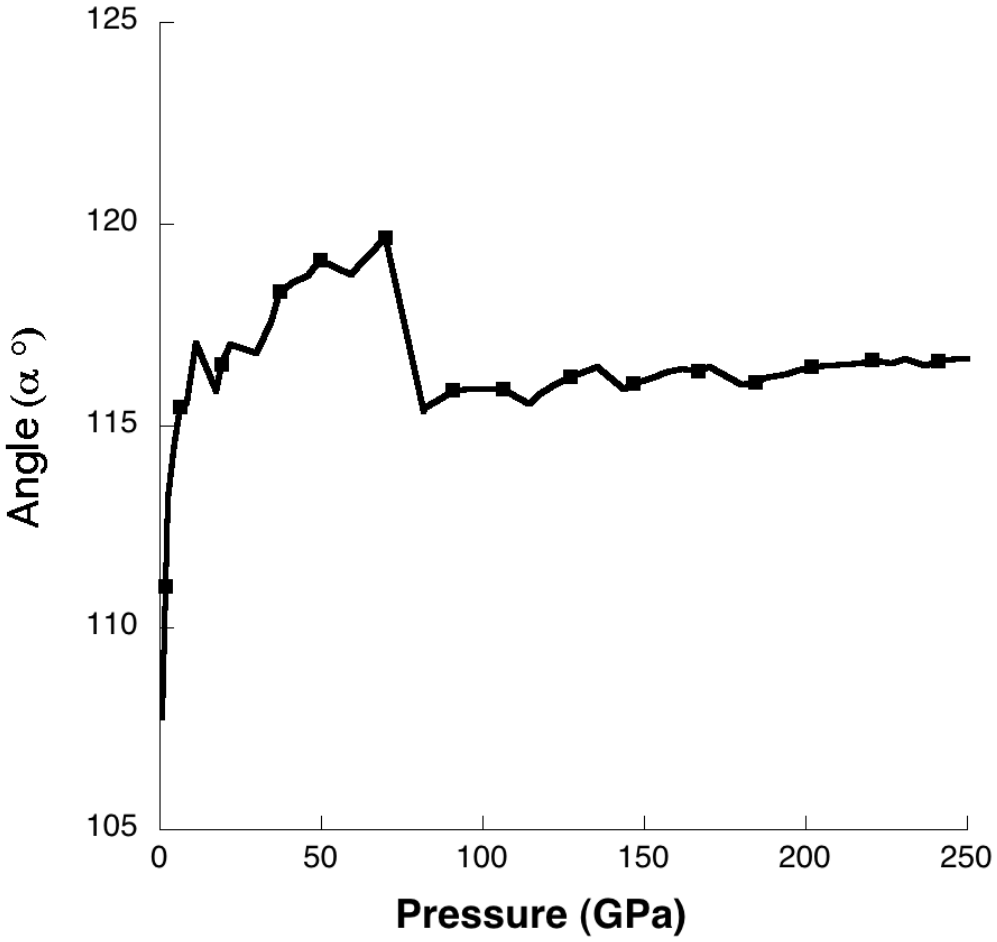

Manaa and Fried: Figure 4 (a).

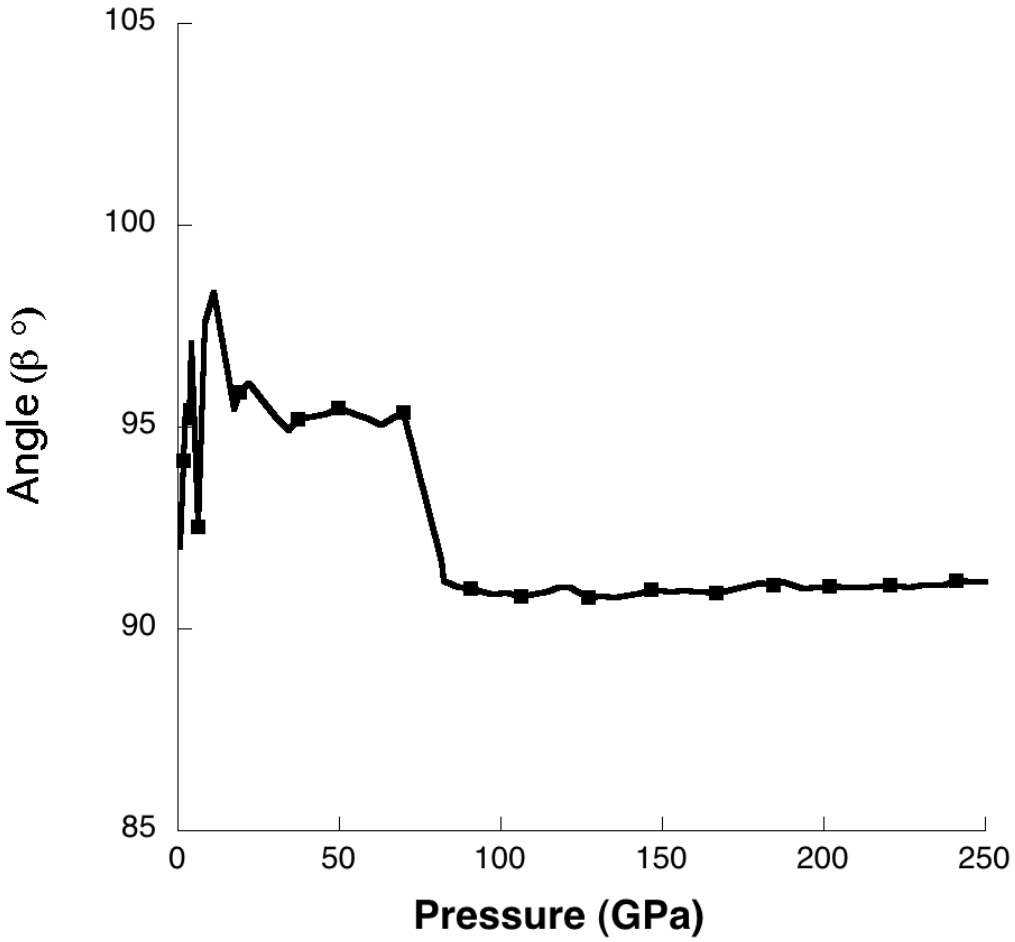

Manaa and Fried: Figure 4 (b).

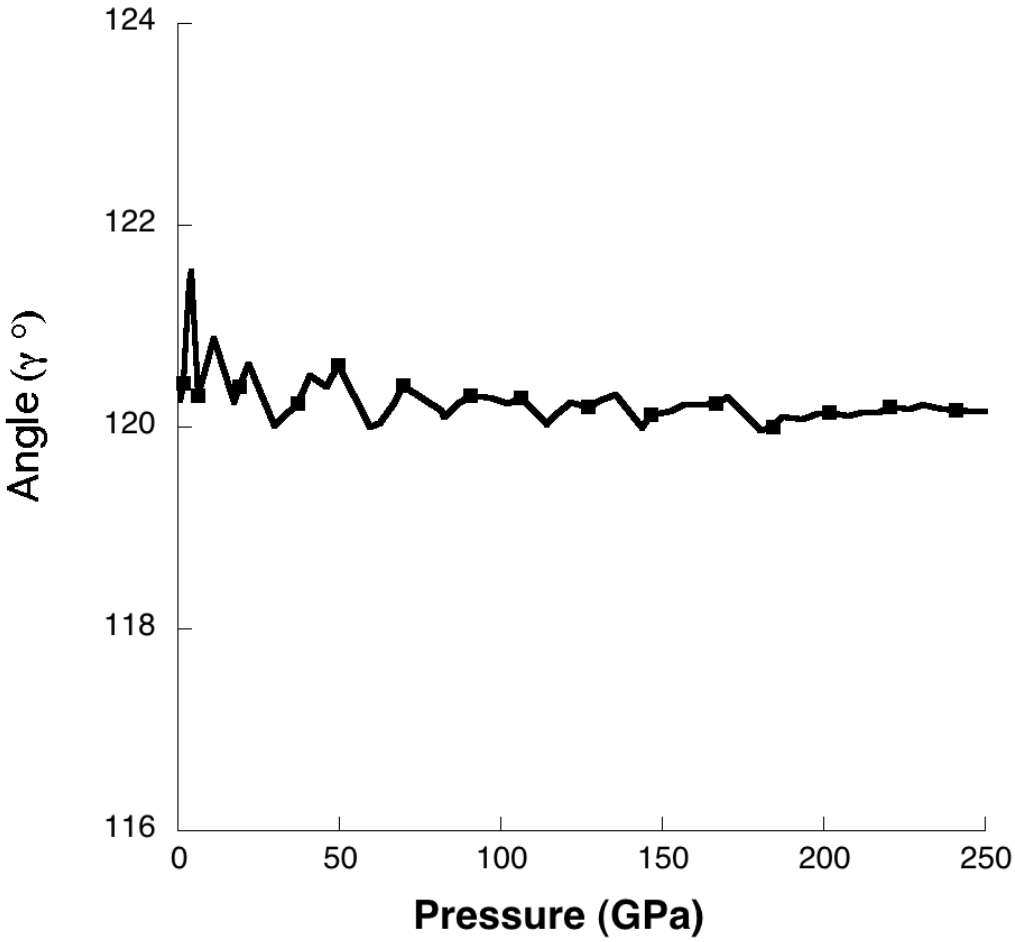

Manaa and Fried: Figure 4 (c).

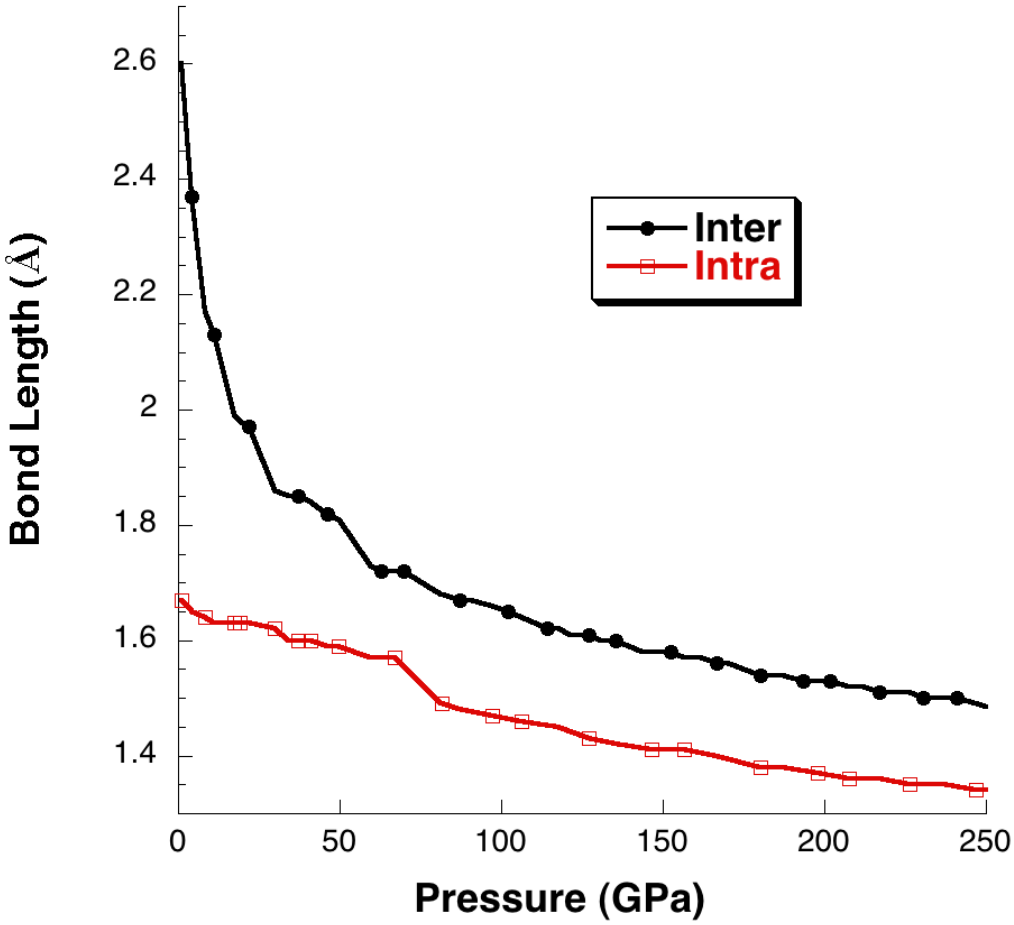

Manaa and Fried: Figure 5.

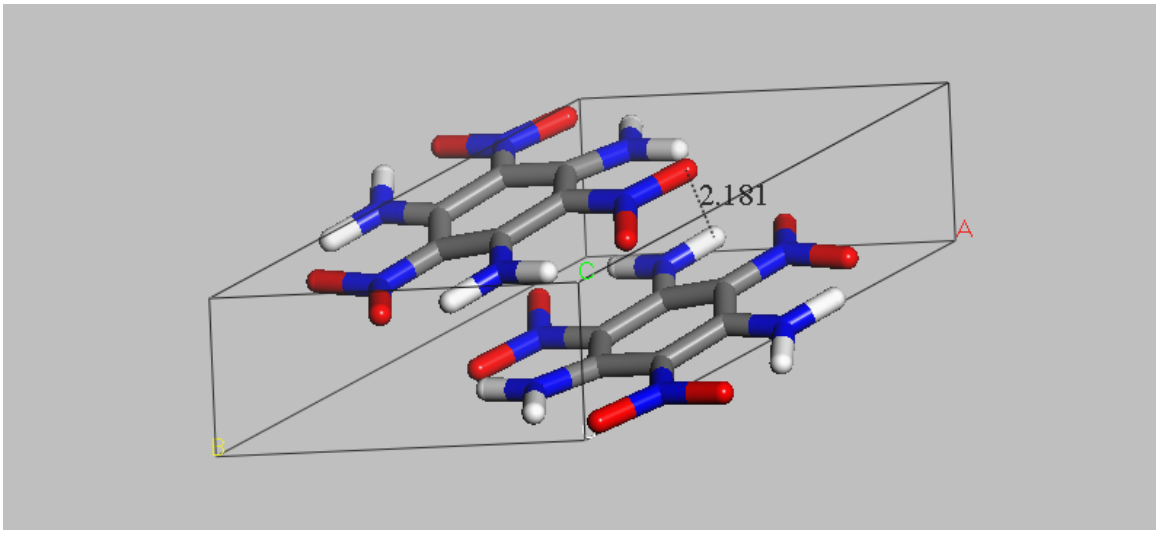

Manaa and Fried: Figure 6a.

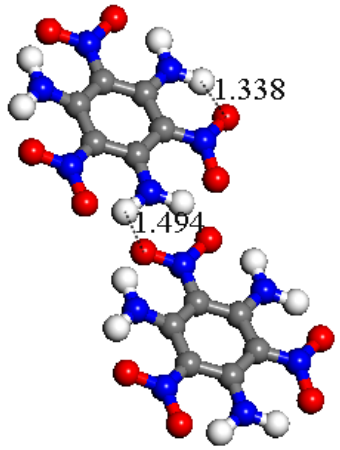

Manaa and Fried: Figure 6b.

References:

(1) Goncharov, A. F.; Manaa, M. R.; Zaug, J. M.; Gee, R. H.; Fried, L. E.; Montgoery, W. B. *Phys. Rev. Lett.* **2005**, *94*, 065505.

(2) Manaa, M. R.; Goldman, N.; Fried, L. E. *Phase Trans.* **2007**, *80*, 1073.

(3) Goldman, N.; Fried, L. E.; Kuo, I. F. W.; Mundy, C. J. *Phys. Rev. Lett.* **2005**, *94*, 217801.

(4) Goldman, N.; Fried, L. E. *J. Chem. Phys.* **2006**, *125*, 044501.

(5) Johannsen, P. G.; Helle, W.; Holzapfel, W. B. *J. Phys.* **1984**, *45*, 199.

(6) Dobratz, B. M. *The Insensitive High Explosive Triminotrinitrobenzene (TATB): Development and Characterization -1888 to 1994*, Los Alamos National Laboratory, 1995.

(7) Cady, H. H.; Larson, A. C. *Acta Crystallogr.* **1965**, *18*, 485.

(8) Foltz, M. F.; Ornellas, D. L.; Pagoria, P. F.; Mitchell, A. R. *J. Mater. Sci.* **1996**, *31*, 1893.

(9) Kolb, J. R.; Rizzo, H. F. *Propellants Explos.* **1979**, *4*, 10.

(10) Manaa, M. R.; Fried, L. E. *J. Phys. Chem. A* **2001**, *105*, 6765.

(11) Manaa, M. R.; Gee, R. H.; Fried, L. E. *J. Phys. Chem. A* **2002**, *106*, 8806.

(12) Gee, R. H.; Roszak, S.; Balasubramanian, K.; Fried, L. E. *J. Chem. Phys.* **2004**, *120*, 7059.

(13) Roszak, S.; Gee, R. H.; Balasubramanian, K.; Fried, L. E. *Chem. Phys. Lett.* **2003**, *374*, 286.

(14) Pravica, M.; Yulga, B.; Liu, Z. X.; Tschauner, O. *Phys. Rev. B* **2007**, *76*, 064102.

(15) Stevens, L. L.; Velisavljevic, N.; Hooks, D. E.; Dattelbaum, D. M. *Prop. Explos. Pyrotech.* **2008**, *33*, 286.

(16) Olinger, B.; Cady, H. In *6th Symposium (International) on Detonation* Coronada, Calfornia, USA, 1976, p 224.

(17) Foltz, M. F. In *13th Symposium (International) on Detonation* Norfolk, Virginia, USA, 2006, p 997.

(18) Satija, S. K.; Swanson, B.; Eckert, J.; Gladstone, J. A. *J. Phys. Chem.* **1991**, *95*, 10103.

(19) Trott, W. M.; Renlund, A. M. *J. Phys. Chem.* **1988**, *92*, 5921.

(20) Pravica, M.; Yulga, B.; Tkachev, S.; Liu, Z. X. *J. Phys. Chem. A* **2009**, *113*, 9133.

(21) Byrd, E. F. C.; Rice, B. M. *J. Phys. Chem. C* **2007**, *111*, 2787.

(22) Liu, H.; Zhao, J.; Du, J.; Gong, Z.; Ji, G.; Wei, D. *Phys. Lett. A* **2007**, *367*, 383.

(23) Sorescu, D. C.; Rice, B. M. *J. Phys. Chem. C* **2010**, *114*, 6734.

(24) Budzevich, M. M.; Landerville, A. C.; Conroy, M. W.; Lin, Y.; Oleynik, I. I.; White, C. T. *J. Appl. Phys.* **2010**, *107*, 113524.

(25) Wu, C. J.; Yang, L. H.; Fried, L. E.; Quenneville, J.; Martinez, T. J. *Phys. Rev. B* **2003**, *67*, 235101.

(26) Perdew, J. P.; Burke, K.; Ernzerhof, M. *Phys. Rev. Lett.* **1997**, *78*, 1396.

(27) Margetis, D.; Kaxiras, E.; Elstner, M.; Frauenheim, T.; Manaa, M. R. *J. Chem. Phys.* **2002**, *117*, 788.
(28) Vanderbilt, D. *Phys. Rev. B* **1990**, *41*, 7892.
(29) Byrd, E. F. C.; Scuseria, G. E.; Chabalowski, C. F. *J. Phys. Chem. B* **2004**, *108*, 13100.
(30) Kresse, G.; Furthmuller, J. *Phys. Rev. B* **1996**, *54*, 11169.
(31) MSI, v.; Inc., A.; v.4.6. ed. San Diego, 1999.
(32) Birch, F. *Phys. Rev.* **1947**, *71*, 809.
(33) Allen, F. H.; Baalham, C. A.; Lommerse, J. P. M.; Raithby, P. R.; Sparr, E. *Acta Cryst.* **1997**, *B53*, 1017.